A Bacteria-Based Remotely Tunable Photonic Device

Mathieu Bennet, Dvir Gur, Jonghee Yoon, YongKeun Park, and Damien Faivre**

Owing to their hierarchical structure, myriad of biological systems exhibit patterns in a size range spanning over more than 10 orders of magnitude. In some instances, these patterns result in striking color effects. For example, some fish and beetles are able to change their color by tuning the periodicity of structures and can inspire the development of tunable photonic devices.[1] However, as opposed to optical materials typically used in photonic devices (e.g., liquid crystals), using these biological materials as a part of a photonic device would be challenging because of their complexity and our inability to control their fabrication and hence control their properties. Alternative to typical optical materials such as liquid crystals exist. For example, Lobov et al. showed how nanofibers can be used as an alternative to liquid crystals.[2] Because of their inherent properties, e.g., size and composition, bacteria are microobjects that interact with light by refracting, reflecting, and absorbing incoming photons and can therefore be used as building blocks for the fabrication of photonic devices.[3] However, in order to fabricate a tunable device, the ordering of the bacteria has to be controllable in a similar fashion to liquid crystals. Magnetotactic bacteria are a group of bacteria that inspire the synthetic fabrication of magnetic nanostructures[4] because they biomineralize magnetic nanoparticles[5] and align them in 1D chains[6] that make them magnetically actuatable. Thus, such bacteria can be packed in an ordered fashion, and the assembly can be remotely controlled using a weak magnetic field. Our study shows how a dense suspension of these bacteria can be used as a tunable photonic device that can control the intensity and phase of the light, offering an alternative to liquid crystal-based technologies.

Magnetospirillum gryphiswaldense (MSR-1) is a spirilla-shaped magnetotactic bacterium that mineralizes magnetite nanoparticles in a membrane (**Figure 1**a). Each cell contains a single chain of 20–30 magnetic nanoparticles (Figure 1b). Figure 1c,d shows the map and 3D reconstruction of the refractive index (RI) of MSR-1 measured by holotomography (HT). From the 3D (RI) tomograms, the mean values of RIs are 1.366 ± 0.008 and 1.360 ± 0.005 for the center and cell wall region of MSR-1, respectively (Figure 1e). An object with a RI of $n_b = 1.366$ suspended in a medium with RI of $n_m = 1.337$ is defined as optically soft since the relation $|m - 1| << 1$ applies, where m is the relative RI given as n_b/n_m. The reflection of an incident wave at the interface of an optically soft particle is negligible.

We formed our device from a dense suspension of these soft objects (see Figure S2, Supporting Information) and tuned its optical properties by aligning the bacteria with an external magnetic field. The alignment of the bacteria in suspension with respect to an applied magnetic field is described by the average cosine of the orientation angle, $\langle \cos \alpha \rangle$. This follows the Langevin equation[7]

$$\langle \cos \alpha \rangle = \coth \frac{\mu B}{kT} - \frac{kT}{\mu B} \tag{1}$$

where μ is the average magnetic moment of a bacterium, B is the magnetic field, k is the Boltzmann's constant, and T is the effective temperature of the system. **Figure 2**a shows the alignment of a suspension of magnetic bacteria as a function of the applied magnetic field.

In order to characterize the optical properties of the suspension as a function of the alignment of the bacteria, the light from three LEDs at 400, 470, and 633 nm is shed sequentially on the sample so that the light propagation direction and the sample plane are perpendicular to each other. Figure 2b shows that as the bacteria are increasingly aligned with the sample plane, the transmitted light increases. The bacteria suspension acts as a tunable optical attenuator.

The data plotted in Figure 2c result from the rotation of the bacteria long axis from parallel to perpendicular to the sample plane. Figure 2c shows that as the bacteria are rotated out of the sample plane, the intensity of transmitted light decreases. Scattering by bacteria is typically calculated using the Rayleigh–Gans approximation (R–G) and/or the anomalous diffraction theorem (ADT).[10] For optically soft objects, the R–G is valid for $x|m - 1| << 1$, and the ADT for $x << 1$, where $x = 2\pi r/\lambda$. In the case of MSR-1, the R–G approximation is not strictly valid, because $x|m - 1|$ is not much smaller than 1. The ADT is also not strictly valid since x is not much greater than 1. MSR-1 are in the intermediate case (IC) for which $|m - 1| << 1$ and $x > 1$.[10,11] The general formula for the scattering efficiency, $Q_{sca,}$ in the IC was derived by Chylek and Li[12] and is given by

$$Q_{sca} = k^2 \, |m - 1|^2 \, \frac{V}{P} \tag{2}$$

Dr. M. Bennet, Dr. D. Faivre
Max-Planck Institute of Colloids and Interfaces
Department of Biomaterials
Science Park, Golm
14424 Potsdam, Germany
E-mail: mathieu.bennet@mpikg.mpg.de;
damien.faivre@mpikg.mpg.de
Dr. D. Gur
Weizmann Institute of Science
Department of Structural Biology
760100 Rehovot, Israel
Dr. J. Yoon, Prof. Y. K. Park
Department of Physics
Korea Advanced Institute of Science and Technology
Daejeon 34141, South Korea
Dr. J. Yoon
Department of Physics
University of Cambridge
Cambridge CB3 0HE, United Kingdom
Prof. Y. K. Park
TOMOCUBE, Inc.
Daejeon 34051, South Korea

DOI: 10.1002/adom.201600617

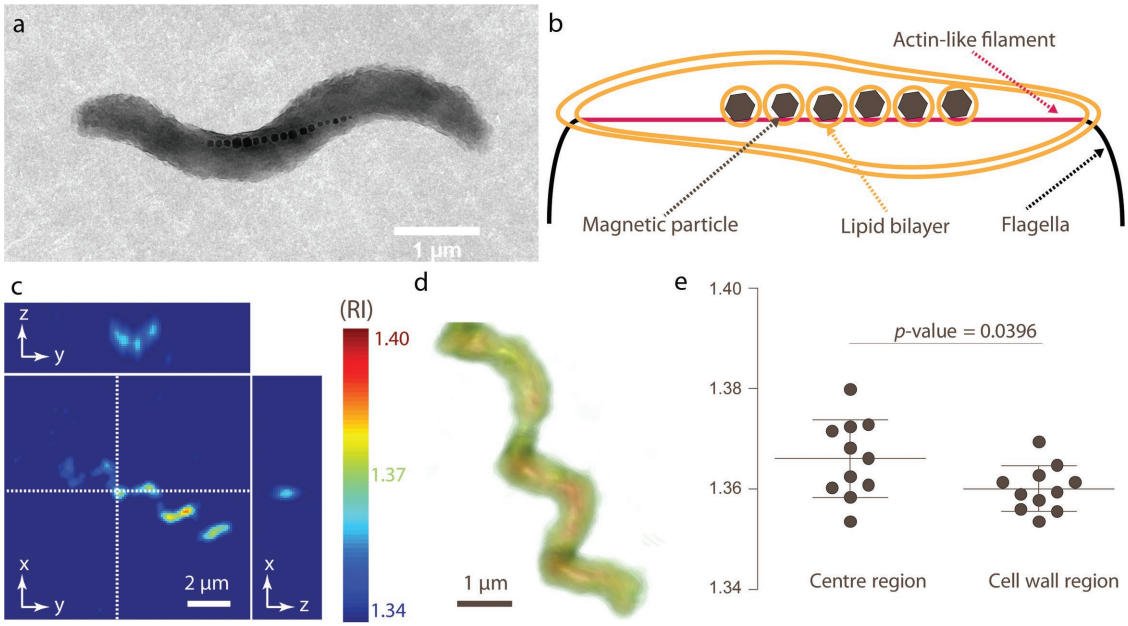

Figure 1. a) Transmission electron microscopy image of a magnetotactic bacterium (MSR-1). b) Simplified schematic of the bacterium showing the magnetic particles contained in lipid vesicles and aligned along an actin-like filament that extends from pole to pole of the cell. c) Cross-sectional slices of a representative 3D RI tomogram. Scale bar is 2 µm. d) A 3D rendered tomogram of a magnetotactic bacterium with customized transfer functions. Scale bar indicates 1 µm. e) Quantification of average RI values according to the central and cell wall region of bacteria. The horizontal and vertical lines indicate the mean value and standard deviation, respectively. The *p*-value indicates statistical analysis RI values in center and cell wall region of bacteria according to Student's *t*-test.

where $k = 2\pi/\lambda$, V is the volume of the scattering object and P is its projection area (PA).

The dependence of the scattering efficiency on the PA explains the data plotted in Figure 2b,c. In Figure 2b, when no magnetic field is applied, the PA is an average for randomly oriented bacteria. As the magnetic field is increased, the PA tends to its maximum and the scattering efficiency tends to its minimum. Figure 2d shows the calculated decrease of the PA of a bacterium as this is rotated out of the sample plane. The PA as a function of the direction of the magnetic field was calculated using models of bacteria made of one to four parallelepipeds (see the Supporting Information). A linear regression between the decrease of the intensity of the transmitted light and the PA for the two- and three-segment model results in a coefficient of determination $R^2 = 0.98$.

Light interaction phenomena other than scattering (i.e., absorption and reflection) can contribute to the behavior shown Figure 2b,c. Absorption is not considered since the light is not linearly polarized and the molecules dipoles in the bacteria are randomly oriented. Reflection in nature can arise from structural materials consisting of layers of alternating refractive indices[13] such as the lipid/magnetite assembly that constitute the magnetic chain in MSR-1. Figure 2e shows that the magnetic chain can lead to a significant reflectance even when the RI difference between the lipid and the nanoparticles is small (Δn = 0.05, R = 0.1). However, at the bacteria density used the probability of an incoming photon to impinge on the chain is ≈0.4%. Therefore the recorded transmitted intensity is not significantly dependent on structural reflection from the magnetic chain.

Next, we realized a setup analogous to a liquid crystal display by placing the suspension between cross-polarizers and assessing the effect of the device on the polarization of the light. The bacteria are oriented in the sample plane and rotated so that the light transmitted through the analyzer is recorded as a function of the angle between the polarizer and the applied magnetic field (i.e., the bacteria). **Figure 3**a shows that as the bacteria are rotated with respect to the polarizer, the intensity of the light transmitted through the analyzer varies, indicating that the bacteria suspension exhibits birefringence. For bacteria, birefringence arises from shape anisotropy and is referred to as form birefringence.[14]

This results from the difference in the phase of the two orthogonal components of forwardly scattered light (Figure 3b and the Supporting Information). Multiple scattering events lead to an accumulation of the phase difference and the formation of a delay, δ, typical of birefringent materials.[14] The birefringence of a bacteria suspension is proportional to the refractive index difference between the bacteria refractive index, n_b, and the refractive index of the medium, n_m, and is given by[15]

$$\Delta n = \frac{f_b f_m (n_b - n_m)}{f_b n_b + f_m n_m} \tag{3}$$

where f_b is the volume fraction of bacteria and f_m is that of the medium. The delay is given by[16]

$$\delta = \frac{2\pi \Delta n d}{\lambda} \tag{4}$$

where d is the physical thickness of the system. For the sample used to generate the data in Figure 3a, Δn = 0.0013, $\delta(400)$ = 5.1, $\delta(470)$ = 4.3, and $\delta(633)$ = 3.2. Figure 3a shows

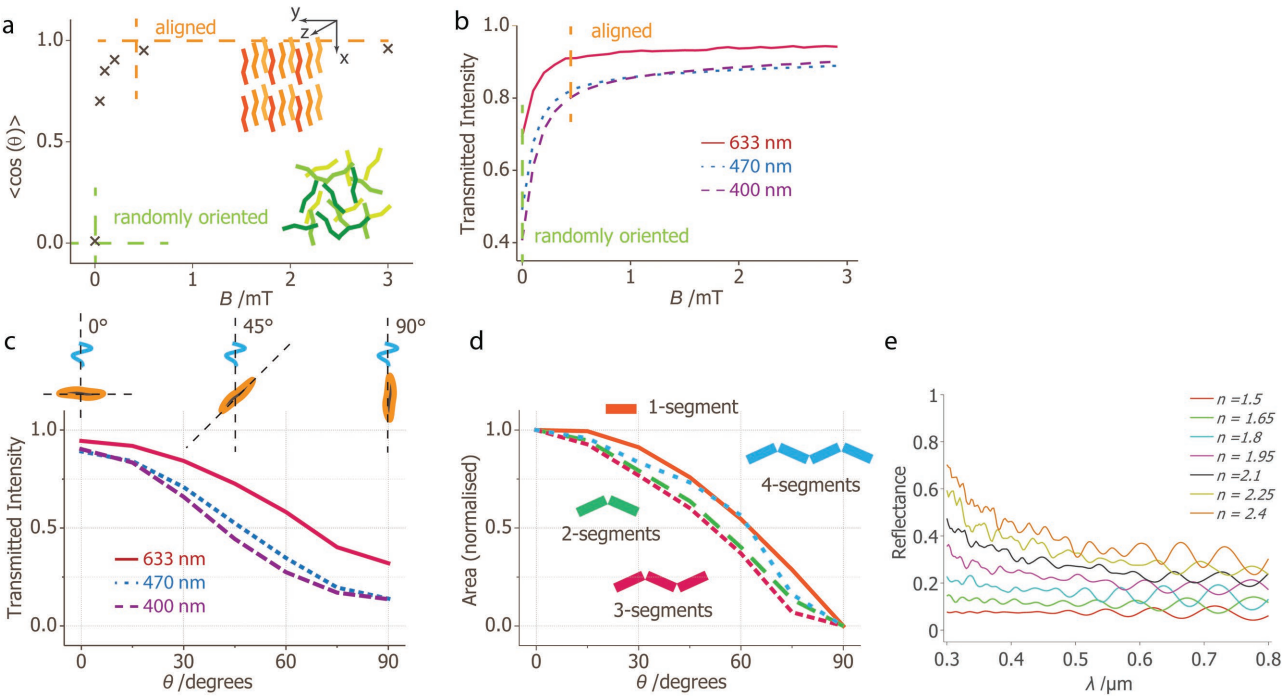

Figure 2. a) Average ($n = 150$) cosine of the angle formed by the bacteria and the magnetic field line, cos (θ), as a function of the applied magnetic field B. b) Corresponding light intensity transmitted as a function of the applied magnetic field. The data are shown for a light-emitting diode (LED) emitting at 633 nm (red line), 470 nm (blue dotted line), and 400 nm (purple dashed line) and a density of 2×10^{10} cells per mL. c) Intensity of the transmitted light as a function of the angle formed by the bacteria long axis and the sample plane. The data are shown for an LED emitting at 633 nm (red line), 470 nm (blue dotted line), and 400 nm (purple dashed line) and a density of 2×10^{10} cells per mL. d) Decrease of the typical length, calculated as the square root of the PA of a bacterium at different angles with respect to the sample plane (see the Supporting Information for calculation details). The PA was calculated for different models of the bacteria. These models are made of one (straight orange line), two (green long dashed line), three (red short dashed line), or four (blue dots) rectangular parallelepipeds at 120° from each other. Models with two and three segments fit best the decrease of the transmitted intensity as a function of angle observed at 633 nm. A linear regression results in a coefficient of determination $R^2 = 0.98$. e) Spectra of the reflectance of the chain of magnetic particles oriented along the light propagation direction. The chain was modeled as a linear assembly of 30 particles 40 ± 5 nm separated by a 10 ± 5 nm layer of lipid. The refractive index of the lipid layer is 1.45. Since the refractive index of magnetite nanoparticles is size and wavelength dependent, the result of the simulation are plotted for a range of refractive indices from $n = 1.5$ (nanoparticles with $d = 12$ nm the reported refractive index is $n = 1.41$[8]) to $n = 2.4$ (for bulk magnetite $n = 2.42$[9]).

that the phase delay is wavelength dependent so that the variations of the transmitted intensities at 400 and 633 nm have different amplitudes. The transmitted intensity at 470 nm has two maxima. This most probably results from the fact that the bacteria suspension has a multiaxial anisotropy.

In summary, a dense suspension of magnetic bacteria was used to fabricate a remotely tunable photonic device. The optical properties of the bacteria-based device are tunable using weak magnetic fields. The scattering efficiency of the device is inversely proportional to the PA of the bacteria on a plane perpendicular to the light propagation direction. As a result, the bacterial orientation modulates the intensity of a light signal, effectively acting as a tunable optical attenuator. In addition, the bacterial suspension is geometrically anisotropic under a magnetic field. It exhibits multiaxial form birefringence and acts as a wave plate the orientation of which can be remotely accessed with an applied magnetic field. In our study, helicoid magnetic bacteria were used. However, photonic devices with different optical properties can be fabricated using microorganisms with a different shape, by staining the bacteria with dyes or expressing fluorescent proteins. In addition, the present work implies that microorganisms can be used for controlling the amplitudes and phase of light such as liquid crystal molecules in display and spatial light modulator technology. Finally, bacteria-based photonic devices can both be upscaled and miniaturized to fit in, e.g., microfluidic devices or hollow core fibers.

Experimental Section

Bacteria Culture and Sample Preparation: Magnetotactic bacteria *M. gryphiswaldense* (MSR-1) were grown to an optical density of 0.25 at 565 nm in a medium as described by Heyen and Schüler.[17] In order to rule out artifacts arising from bacteria motility and growth, these were cross-linked using glutaraldehyde (0.1% vol/vol, CAS No. 111-30-8). These treatments ensured long shelf life and the authors did not observe any changes in the properties of the device over time. The bacteria were then centrifuged at 5000 rpm for 10 min and suspended in a buffer solution containing 4-(2-hydroxyethyl)-1-piperazineethanesulfonic acid (HEPES) (10×10^{-3} M), $NaNO_3$ (4×10^{-3} M), KH_2PO_4 (0.74×10^{-3} M), and $MgSO_4$ (0.6×10^{-3} M) and adjusted to pH 7 using a minute amount of NaOH (10 M). For the measurements, the sample was contained between a microscope slide and a coverslip in air tight double sticky frame (Gene Frame, 25 µL, 1 cm × 1 cm, Thermo Scientific), hence preventing evaporation and ensuring an identical optical path length between samples (see the Supporting Information for schematic).

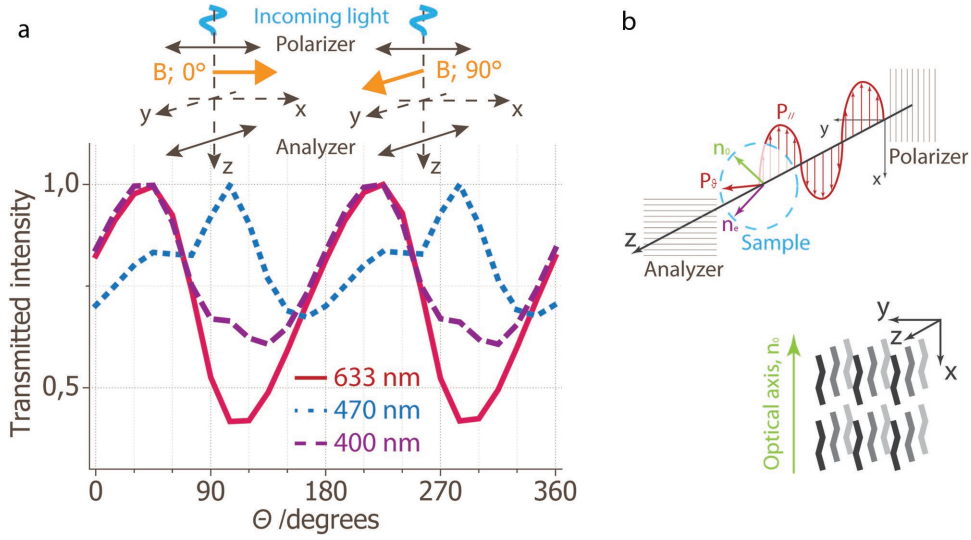

Figure 3. a) Intensity of the light transmitted through a suspension of bacteria as a function of the angle between the bacteria in suspension and the polarizer in a cross polarized setup. The data are shown for an LED emitting at 633 nm (red line), 470 nm (blue dotted line), and 400 nm (purple dashed line) and a density of 6×10^{10} cells per mL. b) Schematic representation of the refractive indices in a birefringent material; light propagation direction in the bacteria suspension; and alignment of the bacteria when the magnetic field is oriented along the *x*-axis, corresponding to the angles 0° and 360° in Figure 3a.

Measurement of Bacteria Alignment: Brightfield optical images of the bacteria were recorded using an objective (60x chromatic aberration-free infinity (CFI) Plan Apo VC 60XWI, Nikon) at various intensities of magnetic fields (0, 50, 100, 500, and 3000 μT). Using ImageJ, the orientation of the bacteria was measured as the angle formed by a line passing through the poles of the bacteria and the magnetic field lines. The average cosine was calculated from the orientation of 150 cells at each magnetic field.

Measurement of the Transmitted Signal: The sample was placed on the sample holder of a microscopy platform equipped with three pairs of Helmholtz coils.[18] Unless indicated otherwise, the magnetic field was set to 3 mT. The illumination was provided by three LEDs emitting at 400, 470, and 633, nm (CoolLED) and the transmitted light was recorded using an sCMOS camera (NeosCMOS, ANDOR) (see the Supporting Information for schematic). In the cross-polarized mode, a polarizer was placed between the light source and the sample holder and an analyzer in front of the camera so that the light detected without a sample was minimized. Each magnetic configuration was applied for 20 s before an image was recorded. The experiment was done once in transmission and once in a cross-polarized mode.

Calculation Reflection from Magnetite/Lipid: Transfer matrix simulations were used to calculate the reflectance of the chain of magnetic particles oriented along the light propagation direction. The mathematical formulation for this method is shown in detail in ref. [19]. In brief, the percent reflectivity was calculated by averaging 300 runs, assuming normal incident light. Every layer was characterized by n_j (refractive index) and d_j (layer thickness). The chain was modeled as an assembly of 30 particles 40 ± 5 nm separated by a 10 ± 5 nm layer of lipid. The refractive index of the lipid layer was taken as 1.45. The refractive index of the magnetite nanoparticles was taken in the range 1.5–2.4. Thus, for each layer the following 2×2 matrix was defined

$$m_j = \begin{pmatrix} \cos\beta_j & -\frac{i}{n_j}\sin\beta_j \\ -i n_j \sin\beta_j & \cos\beta_j \end{pmatrix} \quad \text{where} \quad \beta_j = \frac{2\pi}{\lambda} n_j d_j \tag{5}$$

The set of *k* double layers was characterized by an woverall reflectivity 2×2 matrix

$$M_j = \prod_{j=1}^{j=2k} m_j \tag{6}$$

The reflectivity was extracted from the following expression

$$R = \left| \frac{(m_{11} + m_{12}) - (m_{21} + m_{22})}{(m_{11} + m_{12}) + (m_{21} + m_{22})} \right|^2 \tag{7}$$

The weak dependence of the refractive index on the wavelength was not taken into account when calculating the simulated reflectance and the interface were assumed to be parallel.

Measurements of 3D RI of Magnetotactic Bacteria: 3D RI tomograms of magnetotactic bacteria were measured using a 3D holographic microscope (HT-1S, TOMOCUBE Inc., South Korea).[20] The system consisted of Mach–Zehnder interferometry combined with an active illumination control part that used a digital micromirror device (DMD). A laser beam ($\lambda = 532$ nm) was split into two arms by a 2×2 single mode fiber coupler. One arm was used as a reference beam, and the other arm was reflected by a DMD for varying the angle of the illumination beam impinging onto the sample. 2D holograms were generated by the interference of a sample and a reference beam, which were recorded by a camera. Multiple 2D holograms were recorded for various angles of illumination. For each bacterium, 101 holograms were recorded for reconstructing one 3D RI tomogram via the optical diffraction tomography algorithm. The details of tomogram reconstruction process can be found in previous works.[21]

Supporting Information

Supporting Information is available from the Wiley Online Library or from the author.

Acknowledgements

The authors would like to thank Prof. Peter Fratzl, Prof. Vahid Sandoghdar, and Dr. Richard Taylor for scientific discussions. Financial support from

the National Research Foundation of Korea (2015R1A3A2066550), the European Council (Starting Grant MB2 No. 256915), and from the Max Planck Society is acknowledged.

Received: July 27, 2016
Revised: September 28, 2016
Published online: November 18, 2016

[1] a) D. Gur, B. Leshem, V. Farstey, D. Oron, L. Addadi, S. Weiner, *Adv. Funct. Mater.* **2016**, *26*, 1393; b) A. E. Seago, P. Brady, J.-P. Vigneron, T. D. Schultz, *J. R. Soc., Interface* **2009**, *6*, S165; c) D. Gur, B. A. Palmer, B. Leshem, D. Oron, P. Fratzl, S. Weiner, L. Addadi, *Angew. Chem., Int. Ed.* **2015**, *54*, 12426; d) J. Teyssier, S. V. Saenko, D. van der Marel, M. C. Milinkovitch, *Nat. Commun.* **2015**, *6*, 6368.
[2] G. S. Lobov, Y. Zhao, A. Marinins, M. Yan, J. Li, A. Sugunan, L. Thylén, L. Wosinski, M. Östling, M. S. Toprak, S. Popov, *Adv. Opt. Mater.* **2016**, *4*, 1651.
[3] V. Bianco, V. Marchesano, A. Finizio, M. Paturzo, P. Ferraro, *Opt. Express* **2015**, *23*, 9388.
[4] D. Faivre, M. Bennet, *Nature* **2016**, *535*, 235.
[5] R. Blakemore, *Science* **1975**, *190*, 377.
[6] D. Faivre, T. U. Godec, *Angew. Chem., Int. Ed.* **2015**, *54*, 4728.
[7] R. B. Frankel, *Annu. Rev. Biophys. Bioeng.* **1984**, *13*, 85.
[8] E. Y. Levitin, N. G. Kokodiy, V. A. Timanjuk, I. O. Vedernikova, T. M. Chan, *Inorg. Mater.* **2014**, *50*, 817.
[9] P. Patnaik, *Handbook of Inorganic Chemicals*, McGraw-Hill Professional, New York **2002**.
[10] a) A. L. Koch, *J. Theor. Biol.* **1968**, *18*, 133; b) A. Katz, A. Alimova, M. Xu, P. Gottlieb, E. Rudolph, J. C. Steiner, R. R. Alfano, *Opt. Lett.* **2005**, *30*, 589; c) A. Katz, A. Alimova, M. Xu, E. Rudolph, M. K. Shah, H. E. Savage, R. B. Rosen, S. A. McCormick, R. R. Alfano, *IEEE J. Sel. Top. Quantum Electron.* **2003**, *9*, 277.
[11] M. Xu, M. Lax, R. R. Alfano, *Opt. Lett.* **2003**, *28*, 179.
[12] P. Chylek, J. Li, *Opt. Commun.* **1995**, *117*, 389.
[13] J. N. Lythgoe, J. Shand, *J. Exp. Biol.* **1989**, *141*, 313.
[14] V. V. Tuchin, *Optical Polarizationin Biomedical Applications*, Springer, Berlin **2006**.
[15] R. G. Johnston, S. B. Singham, G. C. Salzman, *Appl. Opt.* **1986**, *25*, 3566.
[16] N. Huse, A. Schonle, S. W. Hell, *J. Biomed. Opt.* **2001**, *6*, 480.
[17] U. Heyen, D. Schüler, *Appl. Microbiol. Biotechnol.* **2003**, *61*, 536.
[18] M. Bennet, A. McCarthy, D. Fix, M. R. Edwards, F. Repp, P. Vach, J. W. C. Dunlop, M. Sitti, G. S. Buller, S. Klumpp, D. Faivre, *PLoS One* **2014**, *9*, e101150.
[19] M. Born, E. Wolf, *Principles of Optics: Electromagnetic Theory of Propagation, Interference and Diffraction of Light*, Cambridge University Press, Cambridge, UK **1999**.
[20] Shin, K. Kim, T. Kim, J. Yoon, K. Hong, J. Park, Y. Park, *Proc. SPIE, Quantitative Phase Imaging II*, **2016**, *9718*, 971814.
[21] K. Kim, H. Yoon, M. Diez-Silva, M. Dao, R. R. Dasari, Y. Park, *J. Biomed. Opt.* **2014**, *19*, 011005.

